



OPEN Effect of biochar and cyanobacteria crust incorporation on soil wind erosion in arid mining area under freeze-thaw action

Zhe Wang^{1,2,5}, Xueshi Liu^{1,5}, Fenghui Sun¹, Qinghong Jiang^{1✉}, Haili Shang³ & Chunli Zheng^{2,4}

The Bayan Obo mining areas of northern China's arid regions is prone to wind erosion and strong freeze-thaw effects. Freezing-thawing leads to the degradation of soil structure and diminishes its resistance to wind erosion. Cyanobacteria crusts can inhibit wind erosion, but their biomass decreases under freeze-thaw conditions. There is limited research on whether combining biochar with cyanobacteria crusts can alleviate the impact of freeze-thaw on their wind erosion resistance. Therefore, the indoor simulated freeze-thaw and wind tunnel tests were used to systematically investigate the impact of cyanobacteria crust and biochar combination on soil wind erosion under freeze-thaw action. Results showed that freeze-thaw cycles altered crust layer soil physicochemical properties. The Pearson correlation coefficient revealed that the freeze-thaw frequency exhibited a significant negative correlation with pH ($p < 0.01$), bulk density ($p < 0.01$), clay percentage ($p < 0.01$), and > 0.25 mm aggregate content ($p < 0.05$). The sensitivity of freeze-thaw cycles to clay percentage was the highest, with a coefficient of variation of 27%. The wind tunnel test showed that the combined use of biochar and cyanobacteria exhibited the most efficient erosion reduction, the erosion reduction rate peaked at a wind speed of 15 m/s, reaching an impressive 64.73%. This was primarily attributed to the high aggregate stability and clay percentage. The above results indicate the biochar and cyanobacteria crust incorporation has great potential as a wind erosion control strategy in seasonal freeze-thaw zones.

Keywords Freezing and thawing, Arid mining area, Biochar, Cyanobacteria crust, Wind erosion

Wind erosion poses a significant environmental challenge¹. China is among the countries heavily impacted by wind erosion, particularly in the arid and semi-arid regions in the north². In regions experiencing severe wind erosion, large-scale open-pit mining activities have resulted in the removal of original vegetation and the destruction of the natural soil structure³. As a consequence, the soil particles become loose and are easily blown away by the wind⁴. Dust and debris generated during excavation, blasting, and transportation in mining also increase the risk of wind erosion⁵. Furthermore, strong winds, low precipitation and soil moisture exacerbate the problem of wind erosion in arid mining areas⁶. Wind erosion in mining areas can lead to the dispersion of pollutants into the surrounding atmosphere, soil, and water environment⁷. These pollutants can then accumulate in the human body through various pathways such as respiration, food chain, drinking water, and skin contact, posing a threat to human health^{8,9}.

Biological crust is a composite soil layer formed by the interaction between algae, lichens, moss, fungi, bacteria, and soil particles on the soil surface¹⁰. The primary succession stage is cyanobacteria crust, which plays a crucial role in the ecosystem of arid and semi-arid areas¹¹. Cyanobacteria can stabilize the soil surface and prevent wind erosion by releasing extracellular polysaccharide substances (EPS) and growing in a filamentous manner¹². However, prolonged formation time, interference from human activities, and lack of soil nutrients

¹School of Energy and Environment, Inner Mongolia University of Science and Technology, Baotou 014010, China.

²Inner Mongolia Engineering Research Center of Evaluation and Restoration in the Mining Ecological Environment, Inner Mongolia University of Science and Technology, Baotou 014010, China. ³School of Mining and Coal, Inner Mongolia University of Science and Technology, Baotou 014010, China. ⁴School of Resources and Environmental Engineering, Shanghai Polytechnic University, Shanghai 201209, China. ⁵Zhe Wang and Xueshi Liu are Co-first authors. ✉email: 19134210@qq.com

and water can significantly delay the natural recovery of cyanobacterial crusts¹³. Therefore, many studies have proposed to accelerate the formation of cyanobacteria crust through artificial inoculation to consolidate sand and resist wind erosion^{14–16}. The establishment of artificial cyanobacteria crusts has led to improvements in soil quality¹⁷, reduction in soil erosion¹⁸, enhancement of soil particle adhesion¹⁶, and increase in carbon sequestration capabilities^{19,20}. However, the instability of the soil surface seriously hinders the successful colonization of artificial cyanobacteria crusts²¹, and the simultaneous inoculation of cyanobacteria crusts and soil stabilizers or amendments may be a promising method for long-term wind erosion mitigation²², which is currently receiving increasing attention^{15,23–25}.

Biochar is a type of insoluble, stable, and highly aromatic carbon containing substance generated by incomplete combustion of biomass under anaerobic conditions²⁶. Biochar exhibits excellent water absorption and retention properties, which can enhance water use efficiency, regulate soil moisture, improve soil fertility, optimize soil structure, increase the stability of soil aggregates^{27–29}. Our previous research has demonstrated that biochar provides multiple pathways for cyanobacteria filaments to cross and extend, while stimulating cyanobacteria to produce more EPS, promoting the cementation of cyanobacteria on soil particles³⁰. Therefore, the technology of combining biochar amendment and cyanobacteria inoculation has significant potential as a wind erosion control strategy. However, under complex climatic conditions, the long-term stability of cyanobacterial crusts–biochar in the natural environment is directly linked to its effectiveness in inhibiting soil wind erosion and diffusion.

Freezing thawing is a natural phenomenon commonly encountered in the soil of arid and semi-arid regions in northern China during late autumn and early spring³¹. It is anticipated that global warming will result in more frequent freeze-thaw cycles in these regions³². These changes in the freeze-thaw cycle can have a significant impact on various soil physical and chemical properties, such as soil bulk density³³, porosity³⁴, soil water content³⁵, soil texture³⁶, aggregate stability³⁷, soil hardness³⁸, organic matter³⁹, total nitrogen content⁴⁰ and others. It leads to the degradation of soil structure and diminishes its resistance to erosion, which provides abundant sand materials for wind erosion in areas with sparse vegetation, dry climate and frequent wind, resulting in a vicious cycle. Due to the fact that cyanobacteria crust is typically found in the top layer of soil profiles, it is more vulnerable to freeze-thaw effects³¹. Previous studies focused on the effects of freeze-thaw cycles on photosynthesis, physiological characteristics, soil nutrient level, hydraulic conductivity, microbial biomass, enzyme activity and ecological function of cyanobacteria crusts^{41–44,21}. The freeze-thaw cycle also decreases the survival rate and the biomass of single cyanobacteria crust, thereby reducing their resistance to wind erosion. Zuo et al.⁴⁵ demonstrated that the application of biochar significantly enhanced the total porosity of soil, facilitated thaw settlement, and mitigated frost heave. In addition, the application of appropriate amounts of biochar alleviated the decreasing trend of aggregate stability and inhibited soil freeze-thaw deformation. However, it remains uncertain whether the incorporation of biochar can mitigate the effects of freeze-thaw cycles on the wind erosion resistance of cyanobacteria crusts in arid mining regions.

Based on this, we assumed that biochar would be beneficial to the resistance of cyanobacteria crusts to wind erosion, even if weakened by freeze-thaw cycles. The aims of this research were to reveal the soil wind erosion reduction mechanism of combined application of cyanobacteria crust and biochar under freeze-thaw action in arid mining area.

Materials and methods

Study area

The Bayan Obo mining area (109°47'–110°04'E, 41°39'–41°53'N) is situated in the southern part of the Mongolian Plateau, within the Inner Mongolia Autonomous Region, China. This region is characterized by an inland dry climate. Due to the influence of strong cold air from regions such as Siberia, Lake Baikal, and Windur Khan, the area experiences low temperatures with minimal rainfall, dry and windy, and the temperature difference is large. The winter is long and cold, up to 7 months, with a minimum temperature of −35.1 °C. The period of freezing occurs from late October to April of the following year, with the depth of frozen soil reaching up to 2.2 m. Spring is characterized by dry conditions and strong sandstorms, often accompanied by powerful winds from March to May, with maximum wind speeds reaching 28 m/s (level 10). Frequent occurrence of freeze-thaw and wind erosion in spring.

Experimental materials

The soil tested was collected from the surface layer (0–10 cm) of the Bayan Obo mining area, with sampling points distributed as uniformly and randomly as possible. After naturally drying the soil used in the experiment, remove impurities such as roots and stones, and sieve it through a 2 mm sieve for later use. The soil is classified as sandy loam, primarily consisting of fine sand particles with a significant presence of non-capillary pores between the particles, resulting in poor soil cohesion.

The species of cyanobacteria utilized in this experiment was *Micrococcus vaginatus*, a type of desert cyanobacteria. *Micrococcus vaginatus* was procured from the Freshwater Algae Culture Collection (FACHB), Institute of Hydrobiology, Wuhan, China, with the designated codes of FACHB-1854. After spread cultivation, the cyanobacteria were filtered from the medium and placed in a constant temperature drying oven, where they were dried at 30 °C until the water content reached about 20%. After drying, they were crushed and set aside.

Using corn stover as the raw material, biochar was prepared through slow pyrolysis at 300 °C, 400 °C, 500 °C and 600 °C for 2 h in a muffle furnace (SK16BYL, Nanjing Boyuntang Instrument Technology Co., Ltd., Nanjing, China). Ultimately, biochar pyrolysis at 400 °C with well-developed pore structure and abundant surface functional groups was selected for further analysis (Fig. S1). Biochar particle size less than 125 µm, passing through a 120-mesh sieve. All biochar samples were stored at 4 °C before further use.

Experimental design

The bare soil from the mine was poured into a 23 cm×12 cm×2.5 cm galvanized tray, ensuring that it filled the tray completely and that the surface of the soil sample was smoothed to create a flat surface. The sample was then divided into four treatment groups, as shown in Table 1. All treatments were replicated three times. The trays were placed in a light incubator with a light intensity of 3000 lx, a light-to-dark period ratio of 12 h:12 h, and a temperature of 25 °C for 60 days. Additionally, 7 mL of distilled water was sprayed daily.

According to the temperature fluctuations and actual freeze-thaw conditions in Baotou, Inner Mongolia, in order to ensure that the soil of each treatment group could be completely frozen and thawed, the freezing temperature was set at −15 °C, and the soil samples were frozen in a refrigerator for 12 h, and then melted at room temperature and thawed for 12 h to simulate the phenomenon of night freezing and day thawing in nature. A total of 30 freeze-thaw cycles were carried out. Part of the samples were taken out for detection at the 0, 5, 10, 20 and 30 cycles, respectively.

Determination of soil physicochemical properties

After freeze-thaw cycles, soil samples (0–2 cm) were taken for the determination of physicochemical properties. Soil pH and electrical conductivity (EC) were assessed using a pH meter (PHS-3 C, China) and an EC meter (4510, Jenway, England), with a soil-to-distilled water ratio of 1:2.5. Total nitrogen (TN) was determined by using the Kjeldahl procedure. Determination of soil water content (SW) by oven-drying method. Soil organic matter (OM) was determined by the potassium dichromate external heating method. The measurement methods of the above indicators are described in the Routine Analysis Method for Soil Agricultural Chemistry as outlined by the Professional Committee of Agricultural Chemistry of the Chinese Society for Soil Sciences⁴⁶. The mechanical composition of the soil was determined by the laser particle size analyzer (Mastersizer 2000, Britain). The aggregates were classified based on their particle size as follows: >2 mm, 1–2 mm, 0.5–1 mm, 0.25–0.5 mm, and <0.25 mm. The water stable aggregate mass for each particle size was determined using the wet sieve method. The content of aggregates larger than 0.25 mm was calculated from the particle size distribution of the aggregates⁴⁷. A cutting ring with a height of 5 cm and a diameter of 5.046 cm was used to sample the top 0–5 cm soil (including the cyanobacterial crust layer) to determine bulk density⁴³. The total porosity of soil was calculated using the bulk density in the Eq. (1). A handheld micro penetrometer (WXGR-2, Cangzhou Taiding Hengye Testing Instrument Co., Ltd, Hebei, China) was utilized to assess the surface strength of soil. The surface strength of the soil can be obtained directly by penetrating the probe vertically into the soil at a constant speed until the line on the probe head contacts the soil surface. Six different points were randomly selected to obtain the surface strength. The insertion of the measuring point had a depth of 20 mm.

Porosity = $\left(1 - \frac{\rho_b}{\rho_s}\right) \times 100$ (1)

where ρ_b is the BD; ρ_s is the density of soil particles, g/cm³, and its average value is generally 2.65 g/cm³.

Wind tunnel experiment

The samples were kept for air drying for 7 days after freeze-thaw cycles⁴⁸, and then tested in the wind tunnel apparatus (AF1300, Beijing Qingshuo Xinye Technology Co., Ltd, Beijing, China). The wind tunnel is 3.7 m long, 1.1 m wide, and 1.9 m high, with a test section of 0.6 m long, 0.3 m wide, and 0.3 m high. The device can produce a maximum wind speed of 36 m/s. The airflow stability coefficient was less than 3.0%, the wind speed uniformity coefficient was 2.0%, the average turbulence was 1%, and the axial static pressure gradient was 0.02/m. The boundary layer thickness of the experimental segment was 80–120 mm. The initial wind speed for soil dust was generally in the range of 4–7 m/s, with few occurrences of wind speeds above level 8 in this area. Therefore, the experiment utilized four different wind speeds: 6 m/s, 9 m/s, 12 m/s, and 15 m/s, corresponding to levels 4, 5, 6, and 7 winds, respectively. The exposure time for each group of soil under different wind speeds was 10 min. The soil samples were weighed before and after wind erosion to calculate the wind erosion intensity and erosion reduction rate (Eqs. 2–4;)⁴⁹. Each experiment was repeated three times, and the average value of the experimental results was used for analysis.

$\omega = m_1 - m_2$ (2)

$E = \frac{\omega}{A \times t}$ (3)

Treatments	Experimental design	Mass ratio
CK	Bare soil in mining area	
C	The dried cyanobacteria were evenly sprinkled on the surface of the mine soil	Soil: cyanobacteria = 20:1
B	The mine soil was mixed with biochar	Soil: biochar = 10:1
CB	Biochar and mine soil were mixed, and then the dried cyanobacteria were evenly sprinkled on its surface	Soil: cyanobacteria: biochar = 20:1:2

Table 1. Experimental groups design.

$$W = \frac{E_0 - E_c}{E_0} \times 100 \quad (4)$$

where ω is mass loss after wind erosion (g); m_1 is the weight of the tray and soil sample before wind erosion (g); m_2 is the weight of the tray and soil sample after wind erosion (g); E is wind erosion intensity ($\text{g}/\text{m}^2\cdot\text{min}$); A is the area of soil sample affected by wind erosion (m^2); t is the wind erosion time (min); W is erosion reduction rate (%); E_0 is wind erosion intensity of CK group ($\text{g}/\text{m}^2\cdot\text{min}$); E_c is wind erosion intensity of other groups ($\text{g}/\text{m}^2\cdot\text{min}$).

Observation of the cyanobacteria crusts microstructure

Field emission scanning electron microscopy (FESEM, MIRA-LMS, Tesken Co., LTD., Czech Republic) was used to observe the surface morphology of cyanobacteria crust and biochar-cyanobacteria crust before and after 30 freeze-thaw cycles at an accelerated voltage of 2 kV.

Statistical analysis

SPSS 23.0 and Origin 2018 were utilized for data statistical analysis and mapping. Specifically, SPSS 23.0 was used to analyze soil physical and chemical indexes (pH, EC, BD, porosity, SW, OM, TN, soil aggregate size distribution and texture), soil surface strength and wind erosion intensity by one-way ANOVA and Person correlation analysis. LSD was used to analyze the significance of test results. The coefficient of variation and relative range were employed to analyze the sensitivity of each factor. Based on statistical principles, the evaluation of soil erodibility sensitivity is categorized into four levels: strong sensitivity (relative range >5 or $\text{CV} > 100\%$), high sensitivity (relative range >2 or $50\% \leq \text{CV} \leq 100\%$), medium sensitivity (relative range >1 or $10\% \leq \text{CV} < 50\%$), and weak sensitivity (relative range <1 or $\text{CV} < 10\%$)⁵⁰. Canoco 5.0 was utilized for conducting redundancy analysis (RDA) to examine the correlation between soil wind erosion intensity and other soil factors constrained by freeze-thaw environment variables. All samples were conducted in triplicate, and the results were the mean \pm standard deviation of the data of the three times.

Results

Effect of freeze-thaw on the microstructure of cyanobacteria crust

FESEM was used to observe the microscopic morphology of cyanobacteria crust (C group) and biochar-cyanobacteria crust (CB group) before and after freeze-thaw (Fig. 1). Before freezing-thawing, the cyanobacteria crust is shown in Fig. 1a. The algal filaments of cyanobacteria weaved soil particles loosely together through the pores between soil particles, which can play a role in fixing the topsoil. The crust of cyanobacteria after the addition of biochar is shown in Fig. 1b. The distribution density of cyanobacterial filaments increased, and a large number of filaments intertwined with biochar and soil particles, indicating that biochar can promote the growth and colonization of cyanobacteria. After 30 freeze-thaw cycles, the distribution density of filaments in the layer soil inoculated only with cyanobacteria decreased, and some cyanobacterial filaments were broken (Fig. 1c), which reduced the ability of cyanobacterial filaments to aggregate soil particles. In the soil with biochar added, the freeze-thaw damage to cyanobacteria was significantly alleviated. The cyanobacterial filaments remained relatively intact without breakage (Fig. 1d).

Changes in physicochemical properties of soil

pH can change the thickness of the “organic coating” on the surface of minerals and the bonding strength between colloidal particles, affecting the formation and stability of soil aggregates, and indirectly impacting the process of wind erosion⁵¹. Conversely, soil wind erosion aggravates the reduction of organic matter and clay migration, resulting in an increase in soil pH⁵². The initial pH values of the CK, B, C, and CB treatment groups were 8.04, 9.01, 7.94, and 8.72, respectively (Fig. 2a). The B treatment group showed an increase of 0.97 units compared to CK, and the CB decreased by 0.29 units compared with group B. After freeze-thaw treatment, the pH value exhibited an overall downward trend, with a more pronounced decrease observed before 20 freeze-thaw cycles. Subsequently, the trend gradually stabilized. After 30 freeze-thaw cycles, the pH values of the CK, B, C, and CB treatment groups decreased by 0.57, 1.70, 0.46, and 1.40 units compared with the initial pH value, respectively.

EC has great influences on soil erosion as well as threshold velocity⁵³. This can be attributed to the effect of soluble and exchangeable cations on soil structural stability through the aggregation or dispersion of soil aggregates⁵⁴. The effect of freeze-thaw on soil EC in different treatment groups was shown in Fig. 2b. The initial EC of CK, B, C and CB treatment groups was 0.77, 0.9, 0.61 and 0.83 mS/cm, respectively. It was observed that the EC of group B and CB was higher than that of CK, while the EC of group C decreased by 20.78% compared to CK. After 30 freeze-thaw cycles, the EC of both the CK and C groups decreased by 19.48% and 37.70%, respectively, compared to the initial EC. The EC of B and CB treatment groups increased by 47.77% and 33.73%, respectively.

Figure 2c showed that the initial bulk density of CK group was $1.28 \text{ g}/\text{cm}^3$, and that of B, C and CB groups was 2.2%, 1.2% and 5.34% lower than that of CK group, respectively, indicating that the addition of biochar and the inoculation of cyanobacteria can significantly reduce the soil bulk density ($p < 0.05$). With the increase of freeze-thaw cycles, the soil bulk density showed a decreasing trend. After 30 freeze-thaw cycles, the CK, B, C, and CB groups decreased by 12.65%, 14.15%, 12.55%, and 10.30% compared to before freeze-thaw, respectively. The treatment group with the addition of biochar exhibited the most significant decrease in bulk density ($p < 0.05$). The impact of freeze-thaw cycles on soil porosity exhibited an opposite trend to that of bulk density (Fig. 2d), with the soil porosity significantly increasing after freeze-thaw compared to before ($p < 0.05$). Specifically, after 30 freeze-thaw cycles, the CK, B, C, and CB groups increased by 6.12%, 6.69%, 6.00%, and 4.72%, respectively.

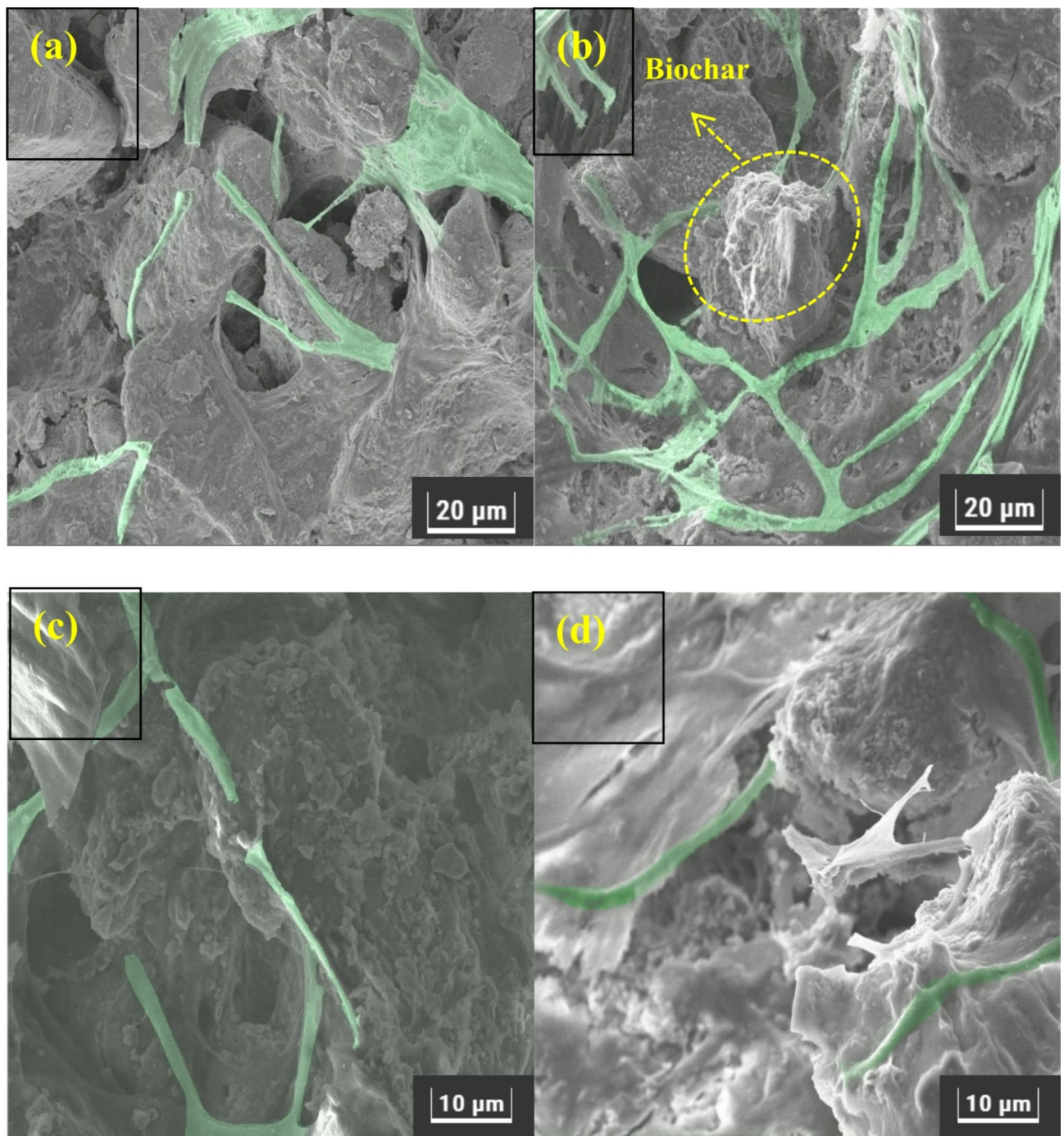


Fig. 1. FESEM images of C (a): before freeze-thaw cycles; (c): after 30 freeze-thaw cycles) and CB group (b): before freeze-thaw cycles; (d): after 30 freeze-thaw cycles).

Before freezing and thawing, the soil water content of CK was 22%. Compared to the CK, the B, C, and CB groups increased by 34.18%, 48.45%, and 68.82%, respectively (Fig. 2e). The CB group demonstrated the highest increase in soil water content. The soil water content of all treatment groups exhibited an increasing trend with the rise in freeze-thaw cycles. After 30 freeze-thaw cycles, the CK, B, C and CB groups increased by 45.59%, 23.01%, 18.86% and 15.97%, respectively. It was evident that the freeze-thaw cycle had the most significant impact on the water content of bare soil.

Soils with elevated TN content typically exhibit improved structure and fertility. A high concentration of organic matter facilitates the formation of soil aggregates, enhances soil stability, and consequently increases resistance to erosion⁵⁵. The soil TN content of different treatment groups is shown in Fig. 2f. TN can improve the nutrient condition of the soil, thereby enhancing its resistance to wind erosion. This process ultimately contributes to the overall health and stability of the soil. Before freeze-thaw cycle, the TN content of CB group was

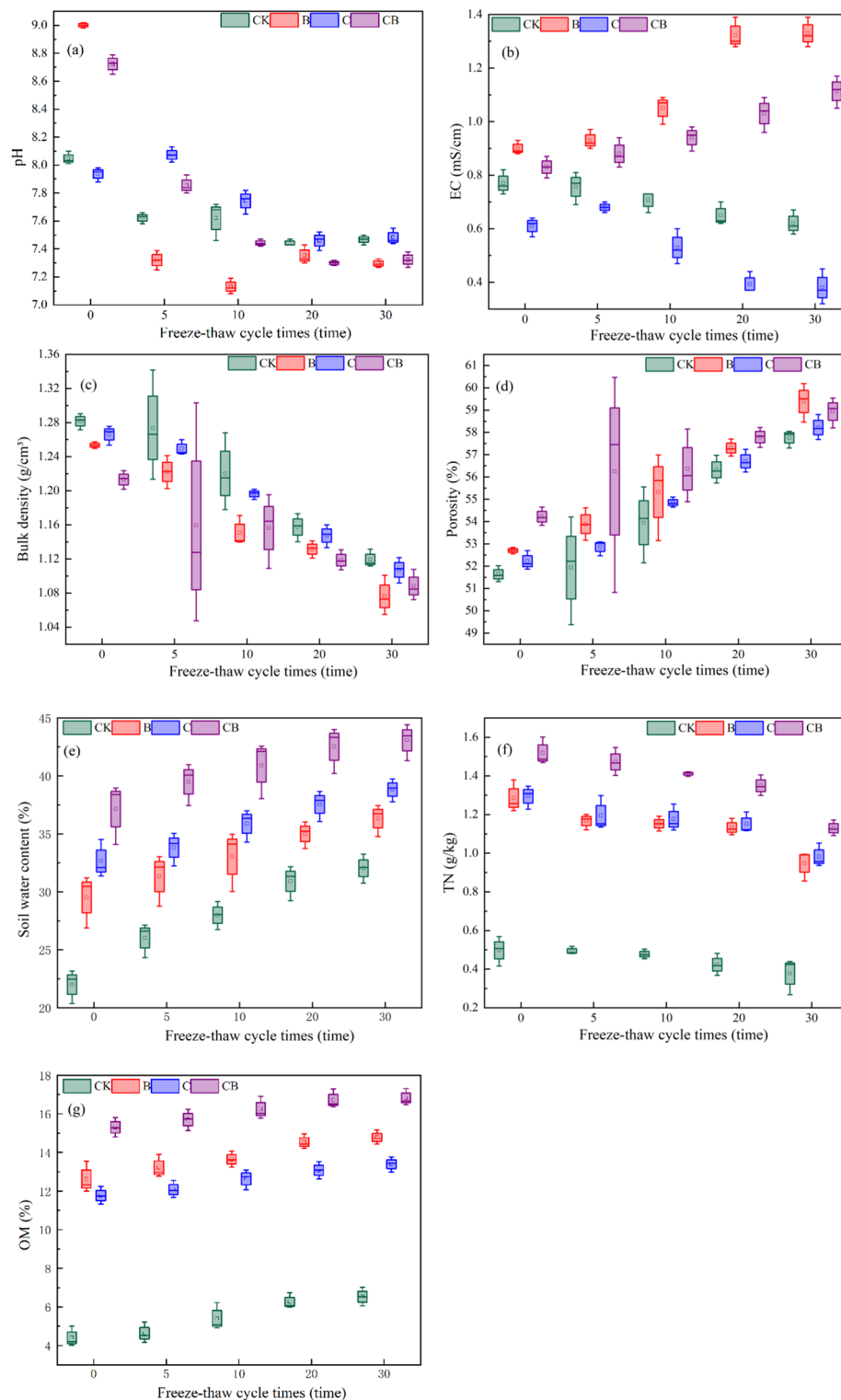


Fig. 2. Effects of freeze-thaw cycles on soil pH (a), EC (b), bulk density (c), porosity (d), soil water content (e), TN (f), and OM (g).

3.06 times that of CK, indicating that the TN content of soil was affected by the synergistic effect of cyanobacteria crust and biochar. After 30 freeze-thaw treatment, soil TN in all groups was significantly decreased ($p < 0.05$). Specifically, compared to levels before the freeze-thaw treatment, the soil TN in CK, B, C and CB groups was decreased by 17.38%, 28.13%, 24.15% and 25.65%, respectively.

Before freeze-thaw, the OM content in group CK was 4.41% (Fig. 2g), and that in group B, C and CB was 1.86, 1.67 and 2.47 times higher than that in group CK, respectively. This indicated that both the addition of biochar

and the inoculation of cyanobacteria would increase the soil OM content. Furthermore, it was evident that there was a synergistic effect between biochar and cyanobacteria which led to the highest OM content in the soil. As the freeze-thaw cycles increased, there was a significant upward trend in the soil OM content ($p < 0.05$). After 30 freeze-thaw cycles, compared to the pre-freeze-thaw period, the OM content in the CK, B, C, and CB groups increased by 48.07%, 17.12%, 13.76%, and 9.93%, respectively. Freeze-thaw had the greatest effect on OM in bare soil.

Before freezing-thawing, the aggregate content of > 2 mm in CK, B, C and CB groups was 41.77%, 48.95%, 46.55% and 54.37%, respectively. The aggregate content of < 0.25 mm was 30.53%, 19.45%, 22.47% and 11.55% for the same groups (Fig. 3a). These results indicated that the addition of biochar and inoculation of cyanobacteria led to an increase in the proportion of macroaggregates and a decrease in the proportion of microaggregates. After the freeze-thaw cycle, the proportion of macroaggregate decreased, while the proportion of microaggregates increased in all treatment groups. Compared with before freeze-thawing, the aggregate content of > 2 mm in CK, B, C and CB groups decreased by 19.08%, 17.19%, 14.75% and 11.49%, while the aggregate content of < 0.25 mm increased by 16.61%, 17.37%, 13.80% and 10.18%, respectively. The freeze-thaw cycle had the least impact on the aggregates of CB group.

According to the soil texture classification standard in the United States, soil particles can be categorized into clay (< 0.002 mm), silt (0.002 – 0.05 mm), and sand (0.05 – 2 mm). The alteration in grain-size distribution affects the mass fraction of sand, silt, and clay present in the soil. The changing of sand, silt and clay particle-size composition in soil during the freeze-thaw process as shown in the Fig. 3b. The soil clay, silt and sand particle-size composition of the CK group before freeze-thaw were 8.30%, 30.35%, and 61.35%, respectively. The CB group exhibited a 28.38% increase in clay and silt particle size composition, while sand particle size composition decreased by 17.88%, compared to the CK group. The percentage of silt in group B increased by 22.16%, while the sand percentage decreased by 13.84%. After 30 freeze-thaw cycles, the sand particle size composition of CK, B, C and CB groups increased by 13.4%, 7.43%, 14.45% and 14.23%, while the silt and clay particle size composition decreased by 21.24%, 8.35%, 21.29% and 14.43%, respectively.

Correlation and sensitivity analysis between freeze-thaw cycle and soil physicochemical properties

Figure 4 shows the correlation analysis between the frequency of freeze-thaw and the physical and chemical properties of soil. The Pearson correlation coefficient revealed that the freeze-thaw frequency exhibited a negative correlation with pH ($p < 0.01$), soil bulk density ($p < 0.01$), soil clay particle size composition ($p < 0.01$), and > 0.25 mm aggregate content ($p < 0.05$). Conversely, it showed a positive correlation with soil porosity ($p < 0.01$), sand particle size composition ($p < 0.05$) and soil water content ($p < 0.05$).

Figure 4 Pearson correlation coefficients matrix of soil pH, electric conductivity (EC), bulk density (BD), organic matter (OM), soil porosity (SP), soil sand particle size composition (SS), soil silt particle size composition (SSI), soil clay particle size composition (SC), soil water content (SW), total nitrogen (TN), > 0.25 mm soil aggregate content ($SA_{>0.25}$). The correlation coefficients were listed in the upper right matrix and the significance were presented in the lower left of matrix. The red color indicates positive correlation, and the blue color indicates negative correlation. The * and ** designates the coefficient is significant at the 0.05 and 0.01 level of probability, respectively.

Correlation analysis was found to be inadequate in reflecting the sensitivity of soil physicochemical properties to freeze-thaw cycles. Therefore, the coefficient of variation and relative range were employed to analyze the sensitivity of each factor in this study (Table S1). The higher the relative range and CV, the greater the corresponding sensitivity level. There were no strong and high sensitivity factors in each treatment group, indicating that freeze-thaw action would not cause drastic changes in each factor. In the CK group, the medium sensitivity factors were SC and $SA_{>0.25}$, OM, EC, and SW. Within group C, the medium sensitivity factors were found to be SC and EC. Moving on to group B, it was observed that the medium sensitivity factors included SC, $SA_{>0.25}$, TN, pH, EC, and SW. Lastly in group CB, the medium sensitivity factors were determined to be SC, EC, and TN. Among the texture factors CK and B, it was found that clay particle size composition exhibited the highest sensitivity, with a CV value reaching 27%. On the other hand, other factors showed weak sensitivity, suggesting that the freeze-thaw cycle had minimal effect on them.

Effect of freeze-thaw on soil surface strength and wind erosion

The soil surface strength after undergoing different freeze-thaw cycles is shown in Fig. S2. The initial surface strength of the CK, B, C, and CB treatment groups were 105.33, 169.45, 176.65, and 243.73 kPa, respectively, with the CB group exhibiting the highest surface strength. This could be attributed to the application of biochar in the soil which promoted the growth of cyanobacteria filaments and the secretion of EPS⁵⁶. As a result, the binding of algal filaments and EPS cementation increased soil stability and led to the formation of stronger soil layers¹⁶. After undergoing 30 freeze-thaw cycles, the surface strength of each treatment group decreased as the number of cycles increased. Specifically, the surface strength of CK, B, C and CB treated groups decreased by 23.25%, 13.17%, 12.13% and 8.03% after 30 freeze-thaw cycles, respectively. This indicated a significant change in soil structure, leading to a looser soil with altered mechanical properties.

The wind erosion intensity of the four groups under different wind speeds are shown in the Fig. 5. Before freeze-thaw, at wind speeds of 6 m/s, 9 m/s, 12 m/s, and 15 m/s, the wind erosion intensities for CK, B, C, and CB groups were as follows: 0.0151, 0.0067, 0.0048 and 0.0007 $\text{kg}\cdot\text{m}^{-2}\cdot\text{h}^{-1}$; 0.4055, 0.1052, 0.0758 and 0.0245 $\text{kg}\cdot\text{m}^{-2}\cdot\text{h}^{-1}$; 0.7614, 0.5576, 0.5445 and 0.4223 $\text{kg}\cdot\text{m}^{-2}\cdot\text{h}^{-1}$; 1.7584, 1.0062, 1.0033 and 0.7287 $\text{kg}\cdot\text{m}^{-2}\cdot\text{h}^{-1}$, respectively. It was found that when the wind speed was less than 9 m/s, the freeze-thaw cycles had a significant effect on wind erosion intensity ($p < 0.05$). However, when the wind speed exceeded 12 m/s, there was no significant difference between 5 freeze-thaw cycles and unfreeze-thaw soils. After 30 freeze-thaw cycles, at wind

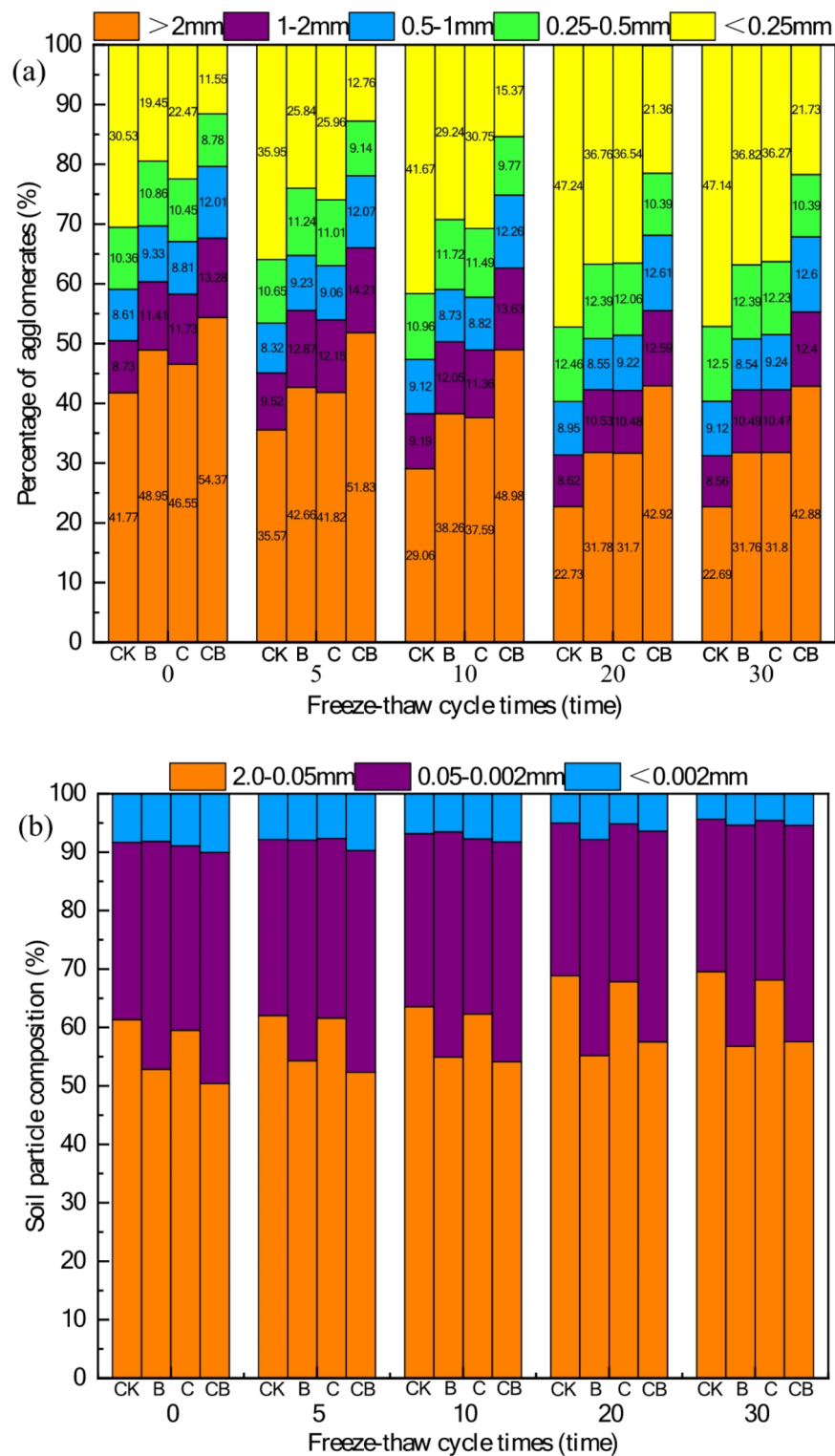
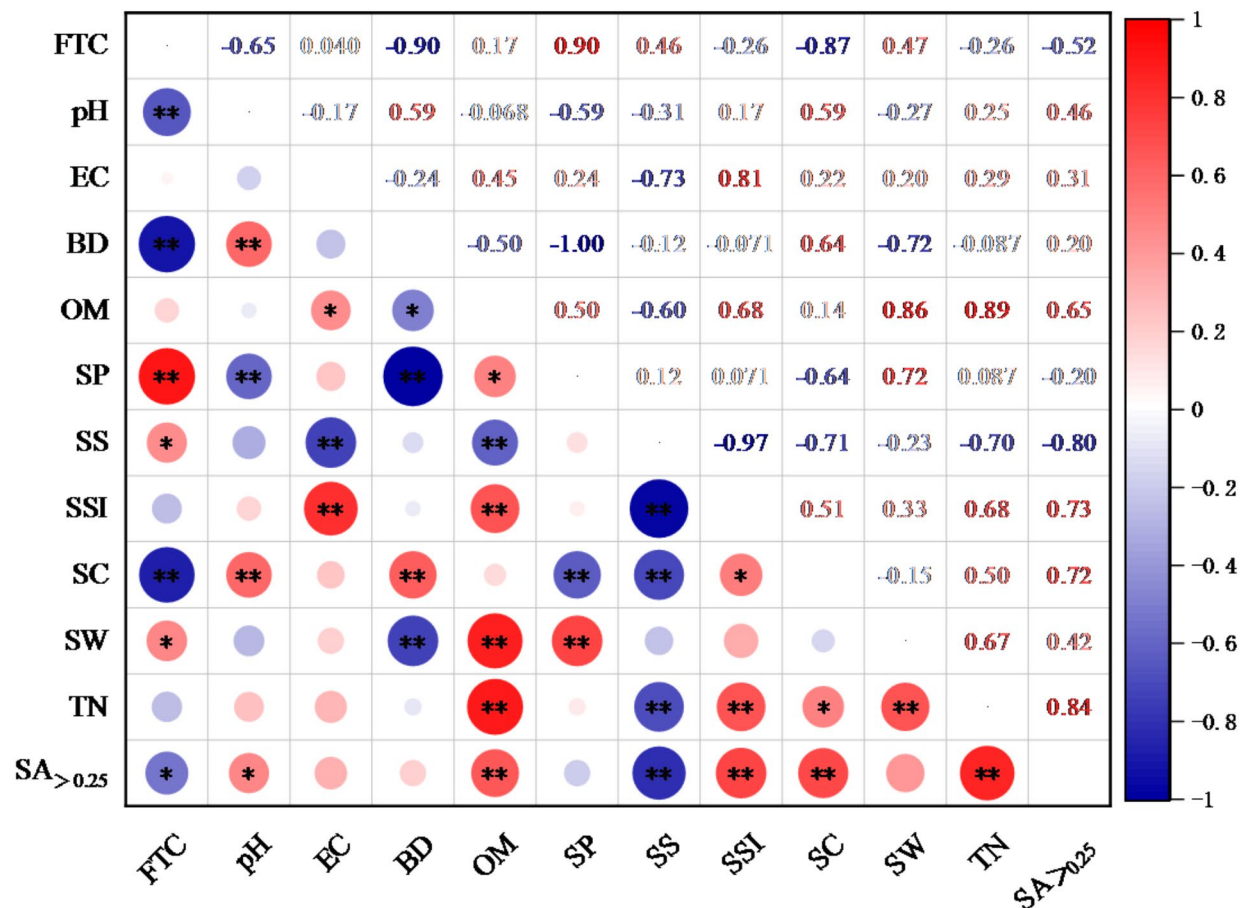


Fig. 3. Effects of freeze-thaw cycles on soil aggregate size distribution (a), and sand, silt and clay particle-size composition (b).



* $p < 0.05$ ** $p < 0.01$

Fig. 4. Pearson correlation coefficients matrix of soil pH, electric conductivity (EC), bulk density (BD), organic matter (OM), soil porosity (SP), soil sand particle size composition (SS), soil silt particle size composition (SSI), soil clay particle size composition (SC), soil water content (SW), total nitrogen (TN), > 0.25 mm soil aggregate content (SA > 0.25). The correlation coefficients were listed in the upper right matrix and the significance were presented in the lower left of matrix. The red color indicates positive correlation, and the blue color indicates negative correlation. The * and ** designates the coefficient is significant at the 0.05 and 0.01 level of probability, respectively.

speeds of 15 m/s, the wind erosion intensity of CK, B, C and CB increased by 1.94, 1.75, 1.76 and 1.65 times compared with that before freeze-thaw, respectively. The freeze-thaw cycle had the most significant influence on the wind erosion of bare soil.

Wind erosion reduction effect of Biochar and cyanobacteria crust incorporation

The erosion reduction rate serves as a crucial parameter for quantifying the impact of freeze-thaw cycles on the wind erosion resistance within each treatment group. In comparison to the CK group, with the exception of the 10 freeze-thaw cycles which showed a higher erosion reduction rate at 12 m/s in the C group, it was observed that the CB group exhibited the most efficient erosion reduction (Table 2). Notably, after undergoing 30 freeze-thaw cycles, the erosion reduction rate peaked at a wind speed of 15 m/s, reaching an impressive 64.73%. These findings suggested that under the influence of freeze-thaw cycles, the CB group demonstrated superior resistance to wind erosion.

The main controlling factors affecting soil wind erosion under freeze-thaw action

Redundancy analysis (RDA) was used to explore the relationship between soil wind erosion intensity and other soil factors constrained by freeze-thaw environment variables. The RDA analysis revealed that RDA 1 and RDA 2 together accounted for a total of 72.46% of the variations. Specifically, RDA 1 explained 41.37% and RDA 2 explained 31.09% of the total variations (Fig. 6).

The results indicated a significant correlation between freeze-thaw and pH, BD, SP, SS, SC, SW, and SA_{>0.25} ($p < 0.05$). This finding was consistent with the Pearson correlation analysis. The intensity of wind erosion showed a significant positive correlation with FTC, SP, and SS because of less than 90° intersection angle ($p < 0.05$).

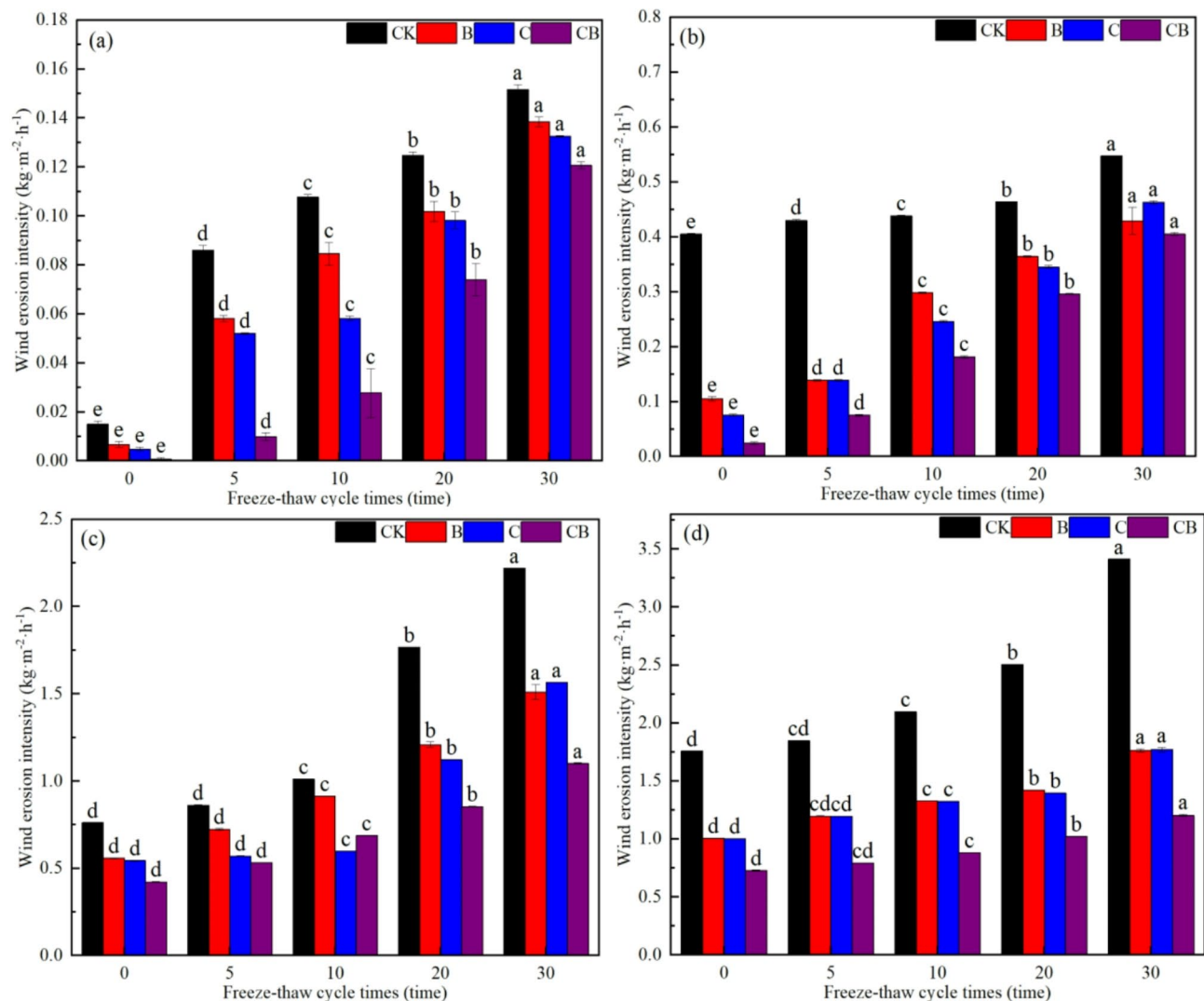


Fig. 5. Effects of freeze-thaw cycles on soil wind erosion intensity at a wind speed of 6 m/s (a), 9 m/s (b), 12 m/s (c), and 15 m/s (d).

Treatments	Wind speed (m/s)	Number of freeze-thaw cycles (times)			
		5	10	20	30
B	6	32.52%	21.45%	18.35%	8.71%
	9	67.67%	31.77%	21.44%	21.60%
	12	15.99%	9.69%	31.60%	31.97%
	15	35.13%	36.72%	43.21%	48.33%
C	6	39.61%	46.05%	21.23%	12.53%
	9	67.74%	43.74%	25.54%	15.42%
	12	33.82%	40.78%	26.46%	29.50%
	15	35.18%	36.86%	44.19%	48.11%
CB	6	88.62%	74.28%	40.79%	20.38%
	9	82.53%	58.57%	36.11%	25.95%
	12	38.23%	31.99%	51.65%	50.45%
	15	56.98%	57.92%	59.16%	64.73%

Table 2. Erosion reducing effect of different treatment groups under freeze-thaw conditions.

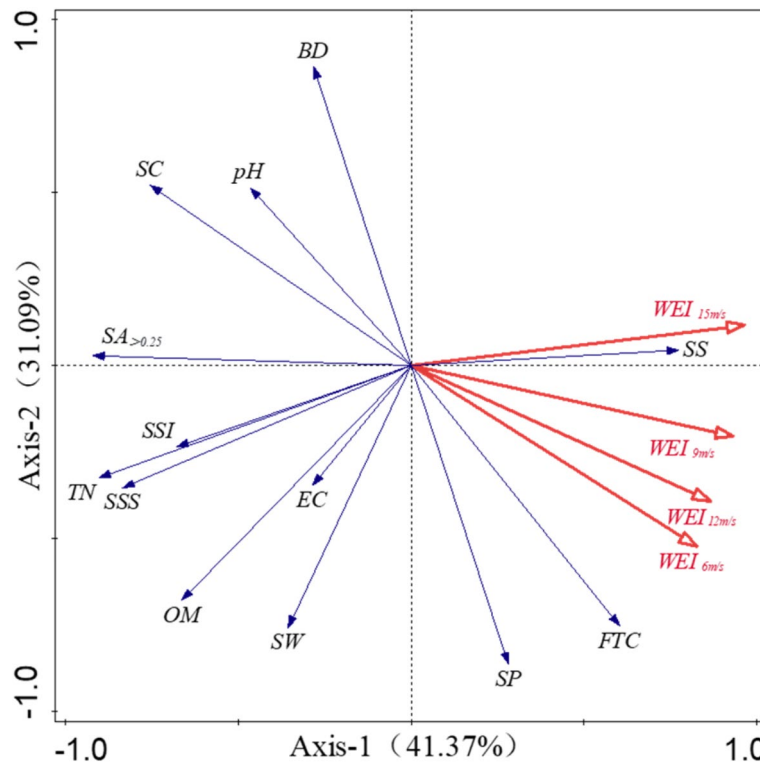


Fig. 6. RDA analysis of the relationship between soil wind erosion intensity ($WEI_{6\text{ m/s}}$, wind erosion intensity of 6 m/s; $WEI_{9\text{ m/s}}$, wind erosion intensity of 9 m/s; $WEI_{12\text{ m/s}}$, wind erosion intensity of 12 m/s; $WEI_{15\text{ m/s}}$, wind erosion intensity of 15 m/s) and other soil factors (EC, electric conductivity; BD, bulk density; OM, organic matter; SP, soil porosity; SS, soil sand particle size composition; SSI, soil silt particle size composition; SC, soil clay particle size composition; SW, soil water content; TN, total nitrogen; $SA_{>0.25}$, >0.25 mm soil aggregate content; SSS, soil surface strength) constrained by freeze-thaw (FTC, freeze-thaw cycle) environment variables.

Contrarily, other factors were negatively correlated with soil wind erosion intensity, as their intersection angles were greater than 90° . At 6 m/s, the order of negative correlation was $SC > SA_{>0.25} > BD > pH > TN > SSS > SSI$. 9 m/s negative correlation was $SA_{>0.25} > SC > TN > SSS > SSI > pH > OM > BD > EC > SW$; 12 m/s negative correlation was $SC > SA_{>0.25} > TN > pH > SSS > BD > SSI > OM > EC$. The negative correlation of 15 m/s was $TN > SA_{>0.25} > SSS > OM > SSI > SC > SW > pH > EC > BD$. The main factors affecting wind erosion intensity at different wind speeds were SC, $SA_{>0.25}$ and TN. It can be seen that the main controlling factors affecting soil wind erosion under freeze-thaw action were soil porosity (positive correlation), sand particle size composition (positive correlation), clay particle size composition (negative correlation) and >0.25 mm soil aggregate content (negative correlation).

Discussion

Effect of freeze-thaw cycles on the physicochemical properties of soil

Freeze-thaw cycles altered soil physicochemical properties. The Pearson correlation coefficient revealed that the freeze-thaw frequency exhibited a significant correlation with pH, soil water content, bulk density, soil porosity, clay particle size composition, sand particle size composition, and >0.25 mm aggregate content. For pH, before freeze-thaw, the addition of fresh biochar can effectively raise soil pH within a short time. This is attributed to the alkaline nature of biochar and its high content of K^+ , Ca^{2+} , and Mg^{2+} ions. Upon application to the soil, these ions are released and exchange with Al^{3+} and H^+ , leading to a reduction in soil acidity (H^+) and an increase in pH⁵⁷. Lin et al.⁵⁸ and Rechberger et al.⁵⁹ both reached similar conclusions. The CB decreased by 0.29 units compared with group B, which may be caused by the addition of biochar inducing the production of more EPS and other small organic acids in the cyanobacteria crust. The freeze-thaw process promoted the nitrification of the soil and the release of dissolved organic acids, leading to a reduction in the pH and an increase in the concentration of H^+ in the soil solution⁶⁰. Among them, the freeze-thaw cycle had the greatest impact on group B. This phenomenon may be attributed to the continuous water and temperature fluctuations during the freeze-thaw cycle, which lead to the dissolution of alkaline minerals in the biochar⁶¹. Furthermore, it is observed that biochar and organic matter in the soil undergo oxidation, resulting in an increase in acidic functional groups during freeze-thaw events. Additionally, it has been noted that organic carbon present on biochar may decompose into low molecular weight organic acids, ultimately leading to a reduction in soil pH⁶².

The soil water content of CB group was the highest before freeze-thaw. The porous structure and high specific surface area of biochar were conducive to water retention⁶³. After the formation of the biological crust through

the inoculation of cyanobacteria, it had been observed that the crust not only had the ability to absorb water, but also effectively reduced water evaporation by blocking surface soil pores⁶⁴. During the freeze-thaw process, soil water content was primarily influenced by soil water potential and ground temperature distribution⁶⁵. As the freezing occurred, water in the soil moved from the lower layer with high water potential to the frozen surface layer with low water potential, resulting in an increase of soil water content in the frozen layer over time. During the thawing process, melted water was transported from the surface layer of soil to the lower layer due to gravity gradient, leading to the accumulation of water in the vertical profile of soil³⁵. As the water content increased during the freeze-thaw process, there was a faster decrease in soil cohesion, which was more likely to result in intensified erosion⁶⁶. In the C and CB groups, the water content changed little during freeze-thaw process. This was due to the covering effect of the crust, which hindered heat loss during freezing and inhibited water evaporation during thawing. As a result, there was a strong regulatory effect on liquid water and temperature.

The addition of biochar and the inoculation of cyanobacteria can reduce the soil bulk density and increase porosity. The biochar had a relatively low density, and its porous characteristics and larger specific surface area were beneficial for improving porosity, thereby reducing soil bulk density⁶⁷. Additionally, the dilution effect of biochar and the reduction of soil mass per unit volume can also contribute to the decrease in soil bulk density⁶⁸. Obia et al.⁶⁹ also showed that the accumulation of soil macrosediment caused by biochar had a direct dilution effect on soil bulk density. After inoculation with cyanobacteria, the lower bulk density of biocrust soil may be attributed to higher organic carbon content, improved soil aggregation and reduced compaction⁷⁰. Frequent phase transitions of soil moisture disrupted the original spatial arrangement of soil particles during freeze-thaw cycles. The growth of ice crystals and the formation of aggregates between ice crystals and soil particles during the cementation process increased pore area, compressed soil particles, and increased porosity, leading to a decrease in soil bulk density⁷¹. Although the ice crystals melt during thawing, the deformation of the soil was not fully recovered⁷². The B group exhibited the most significant change ($p < 0.05$). After the addition of biochar to the soil, the water absorbed in the pores of the biochar expanded during the freezing process, leading to rupture of the biochar particles and a decrease in their size. The resulting small-size biochar particles will fill into the soil macropores, creating a large number of small and medium-sized pores, thereby increasing the total porosity and decreasing soil bulk density^{73,74}.

The alternating freeze-thaw cycles can cause intense contraction and expansion of pore spaces within and between soil aggregates. The macroaggregates possess larger pore space and better structural stability, which helps to reduce soil wind erosion and enhance water retention⁷⁵. As a result of macroaggregate breakage, microaggregates were newly formed through soil deformation compression and soil water adsorption⁷¹. Specifically, the freeze-thaw cycle altered the internal structure of aggregates, leading to increased porosity, asymmetric pores, and tubular pores, ultimately affecting aggregate stability⁷⁶. Under freeze-thaw action, there will be significant changes in soil sand, silt and clay particle-size composition due to energy input and output, as well as water and salt transport. Zhang et al.⁷⁷ found that when the degree of freeze-thaw reached a certain threshold, the coarse mineral particles, including sand and silt particles would be fractured. Due to the presence of a significant amount of water molecules surrounding the clay particles in the form of bound water, they were not susceptible to freezing under general freeze-thaw conditions. Consequently, the structure of the clay particles remained intact and was not destroyed, which was inconsistent with the result of this study. In this study, it was observed that the particle size distribution of clay and silt decreased following freeze-thaw cycles, while the particle size distribution of sand increased. This phenomenon may be attributed to the silt particles are used as the core, and clay particles are used as the inclusion to aggregate into sand particles. This process results in a reduction in the particle size percent of silt and clay, accompanied by an increase of sand⁷⁸. In addition, soil porosity increases after freeze-thaw, and fine clay and silt particles may move down with water during freeze-thaw process, resulting in a relative decrease in particle size percent.

Although TN and OM did not show a significant correlation with freeze-thaw cycles, they still underwent changes during this process. Freezing of the soil can inhibit the diffusion of oxygen, creating an anaerobic environment that enhances denitrification and accelerates the loss of nitrogen in the soil. Additionally, water infiltration resulting from soil melting further contributes to the loss of inorganic nitrogen. As a result, the freeze-thaw cycle had been found to significantly decrease soil TN levels⁷⁹. After inoculation of cyanobacteria, the soil of C and CB groups experienced a rapid decrease in free water within the cyanobacteria cells when the temperature dropped below 0 °C, potentially leading to loss of certain cellular functions. The damage degree of the biological crust at low temperatures was found to be greater than that of the soil layer, leading to a decrease in the TN content of the crust⁴⁴. In addition, group B experienced the greatest decrease in TN during the freeze-thaw process, which may be due to the decreased stability and more severe fragmentation of soil aggregates after adding biochar. The release of a large amount of organic nitrogen reduced the abundance of the nitrogen fixing gene *nifH*⁸⁰.

The repeated expansion and contraction of water caused by freeze-thaw cycle caused the greatest damage to bare soil aggregates, organic and inorganic colloids, and the increase of fine particles with large specific surface area promoted the adsorption of OM, leading to the redistribution and dissolution of OM⁸¹. In addition, the freeze-thaw cycle destroyed the binding of OM and soil particles, which also led to increased OM release³⁹. The freeze-thaw cycle increased the mortality of cyanobacteria crust and further promoted the accumulation of OM and nutrients⁸². The freeze-thaw cycle caused certain fragmentation of the pore structure of biochar, and more small pores can store OM, limiting the decomposition of OM by microorganisms, thereby increasing the content of OM⁸³.

The soil wind erosion reduction mechanism of combined application of cyanobacteria crust and biochar under freeze-thaw action.

During the process of freeze-thaw, the frequent phase transition of water among soil particles resulted in the deterioration of tensile force. As the water within the soil expanded during freezing, it exerted significant stress

on the microporous structure of the soil, leading to an increase in inter-particle spacing. Upon thawing, some of these expanded pores were unable to fully revert back to their original state, thereby compromising the cohesion between soil particles and consequently diminishing both adhesion and compressive strength⁸⁴. Consequently, this deterioration in soil structure contributed to an escalation in wind erosion.

The presence of crust clearly reduced wind erosion intensity in soil. During growth, cyanobacteria crusts can secrete EPS, which aggregated soil particles and compacted the soil surface, thereby increasing its resistance to wind erosion. Additionally, cyanobacteria filaments can entangle loose particles on the soil surface to form a stable soil matrix that effectively resists wind erosion⁸⁵. The freeze-thaw cycle may cause the cyanobacteria filaments to break, thus weakening the binding to soil particles, as confirmed by Fig. 1c. Biochar possesses a low thermal conductivity, high specific surface area, and porosity. When applied to soil, biochar increases the total porosity of the soil and enhances the content of mechanically stable aggregates and water-stable aggregates. Consequently, this leads to an increase in pore diameter and gas within the unit volume of soil, which impedes heat transfer⁸⁶. As a result, it reduces the thermal conductivity of soil and minimizes fluctuations in soil temperature⁸⁷. This temperature regulation effect of biochar can alleviate damage caused by freezing and thawing to cyanobacteria filaments. EPS plays a crucial role in enhancing the stability and resistance to adversity of biological crust⁸⁸. The content and physical and chemical properties of EPS are influenced by various factors such as temperature and environmental conditions during the growth of crust⁸⁹. In harsh environments characterized by frequent freeze-thaw cycles, cyanobacteria crusts tend to utilize fixed organic carbon to synthesize more EPS in order to cope with environmental stress⁹⁰. In addition, previous research had also indicated that under the stimulation of biochar, cyanobacteria secreted a higher number of EPS with α -polysaccharide as the main component. Consequently, crusts formed through biochar treatment exhibited greater resistance to freeze-thaw interference.

RDA revealed that the primary factor influencing soil wind erosion under freeze-thaw action was the soil clay particle size composition and >0.25 mm aggregate content, with a negative correlation. The soil clay particle size composition and >0.25 mm aggregate content of each group showed a significant decrease with an increase in freeze-thaw cycles ($p < 0.05$). After 30 freeze-thaw cycles, the soil clay particle size composition and >0.25 mm aggregate content in the CK, B, C, and CB groups were 4.38%, 5.37%, 4.56% and 5.40%; 52.86%, 63.18%, 63.73% and 78.27%, respectively. It was worth noting that the CB group exhibited the highest levels of these indexes. Soil texture is a relatively stable characteristic of soil that typically evolves over geological time scales. However, the redistribution of particles within shorter time frames can alter soil texture⁹¹. In fact, particle size distribution has undergone slight changes with the development of cyanobacteria crusts. Compared with bare soil, clay was enriched when cyanobacteria crust was present, while the sand particle size composition was lower than when cyanobacterial crusts were absent. This may be because cyanobacteria crusts can roughen surfaces and exude gelatinous EPS, causing fine particles from the air to be trapped, with clay concentrating on the soil surface in the process⁹². Biochar has abundant pores and huge specific surface area, which can provide a large number of adsorption sites for soil particles, including clay particles, so that clay particles are more easily attached and not easily carried away by wind or water⁹³. The synergistic effect of biochar and cyanobacterial crusts enhances the clay particle size composition in soil. Clay possesses a high-water retention capacity, enabling it to retain moisture during freeze-thaw cycles⁹⁴. Moderate moisture levels can strengthen the cohesion among soil particles, leading to the formation of a more stable structure. This stability mitigates the development of cracks and pores resulting from freezing and thawing processes, thereby reducing wind erosion effects on the soil.

Aggregates are the fundamental components of soil structure, consisting of porous formations created by mineral particles and organic matter through the action of cementitious substances⁹⁵. The stability of soil aggregates is crucial, as it indicates the ability of soil structure to maintain its original state when subjected to external forces and environmental changes. This stability serves as a key indicator of soil erosion resistance⁹⁶. Freezing and thawing can lead to the breakdown of the bonding force between particles in soil aggregates, thereby reducing their resistance to wind erosion. Biochar in the CB group has the ability to increase the organic carbon content in soil. Organic carbon serves as a crucial binding material, which can improve the aggregation of soil particles and facilitate the formation of aggregate structures⁹⁷. Cyanobacteria crusts play a significant role in contributing large amounts of organic carbon to the soil. This is achieved through carbon sequestration and the decomposition of organic matter, both of which are essential for the formation of aggregates⁹¹. The EPS produced by cyanobacteria serves as a cementing agent, closely bonding with clay particles in the aggregates and promoting the formation of large soil aggregates. Additionally, algal filaments can create a network structure that encloses microaggregates and mineral particles, thereby contributing to the formation of larger aggregates⁹⁸. In addition, the surface of biochar contains a large number of oxygen-containing functional groups, such as hydroxyl (–OH) and carboxylic (–COOH) groups. EPS secreted by cyanobacteria is a substance rich in polysaccharides, proteins and other biological macromolecules, in which hydroxyl, amino (–NH₂) and other groups can form a relatively stable bond with the oxygen-containing functional groups on the surface of biochar through hydrogen bonding⁹⁹. This interaction enhances the cohesion between soil particles and significantly improves the stability of aggregates. During freeze-thaw cycles, these stable aggregates are less susceptible to destruction, thereby reducing the exposure and dispersion of soil particles and consequently diminishing the potential for wind erosion.

In conclusion, the incorporation of biochar into the cyanobacteria crust soil further enhanced the soil's resistance to wind erosion. This was attributed to the fact that adding biochar alleviated damage caused by freezing and thawing to cyanobacteria, enhanced aggregate stability and improved soil texture. As a result, the soil was better protected from wind effects under freeze-thaw action.

Conclusions

The freeze-thaw cycle had a significant impact on various soil physical and chemical properties. After 30 freeze-thaw cycles, the pH, bulk density, and TN of all treatment groups decreased. In contrast, the porosity,

aggregate content of < 0.25 mm, sand percentage, OM, and soil water content increased. The Pearson correlation coefficient revealed that the freeze-thaw frequency exhibited a negative correlation with pH, soil bulk density, soil clay percentage, and > 0.25 mm aggregate content. Conversely, it showed a positive correlation with soil porosity, sand percentage and soil water content. The coefficient of variation and relative range showed that clay percentage exhibited the highest sensitivity, with a CV value reaching 27%. After 30 freeze-thaw cycles, the wind erosion intensities of CK, B, C and CB groups increased significantly with the increase of freeze-thaw times ($p < 0.05$). CB group exhibited the most efficient erosion reduction, the erosion reduction rate peaked at a wind speed of 15 m/s, reaching an impressive 64.73%. These findings showed that the CB group exhibited excellent wind erosion resistance under the influence of freeze-thaw cycles, which was attributed to the fact that adding biochar alleviated damage caused by freezing and thawing to cyanobacteria, enhanced aggregate stability and improved soil texture. This study can provide a theoretical basis for controlling soil wind erosion in dry mining areas during the seasonal freeze-thaw period.

Data availability

The data used to support the findings of this study are included within the article and the supplementary information files.

Received: 6 September 2024; Accepted: 31 March 2025

Published online: 11 May 2025

References

- Shen, Y. P., Zhang, C. L., Wang, X. S., Zou, X. Y. & Kang, L. Q. Statistical characteristics of wind erosion events in the erosion area of Northern China. *Catena* **167**, 399–410. <https://doi.org/10.1016/j.catena.2018.05.020> (2018).
- Li, Z. D. et al. The trend shift caused by ecological restoration accelerates the vegetation greening of China's drylands since the 1980s. *Environ. Res. Lett.* **17**, 044062. <https://doi.org/10.1088/1748-9326/ac6002> (2022).
- Liang, J. et al. Impacts of Large-scale rare Earth mining on surface runoff, groundwater, and evapotranspiration: A case study using SWAT for the Taojiang river basin in Southern China. *Mine Water Environ.* **38**, 268–280. <https://doi.org/10.1007/s10230-018-00587-w> (2019).
- Liu, T. & Liu, S. The impacts of coal dust on miners' health: A review. *Environ. Res.* **190**, 109849. <https://doi.org/10.1016/j.envres.2020.109849> (2020).
- Bao, Q. et al. The preparation of a novel hydrogel based on crosslinked polymers for suppressing coal dusts. *J. Clean. Prod.* **249**, 119343. <https://doi.org/10.1016/j.jclepro.2019.119343> (2020).
- Zhang, X. et al. Research on performance of composite dust suppressant for mining based on modified soybean protein isolate. *Powder Technol.* **415**, 118166. <https://doi.org/10.1016/j.powtec.2022.118166> (2023).
- Wang, D. et al. Interaction of Biochar with extracellular polymers of resistant bacteria restrains Pb(II) adsorption onto their composite: Macro and micro scale investigations. *Bioresour. Technol.* **44**, 131602. <https://doi.org/10.1016/j.biortech.2024.131602> (2024).
- Zhou, L. et al. Evaluating of the performance of a composite wetting dust suppressant on lignite dust. *Powder Technol.* **339**, 882–893. <https://doi.org/10.1016/j.powtec.2018.08.081> (2018).
- Wang, Z. et al. Annual dust pollution characteristics and its prevention and control for environmental protection in surface mines. *Sci. Total Environ.* **825**, 153949. <https://doi.org/10.1016/j.scitotenv.2022.153949> (2022).
- Elbert, W. et al. Contribution of cryptogamic covers to the global cycles of carbon and nitrogen. *Nat. Geosci.* **5**, 459–462. <https://doi.org/10.1038/ngeo1486> (2012).
- Xiao, B., Hu, K. L., Ren, T. S. & Li, B. G. Moss-dominated biological soil crusts significantly influence soil moisture and temperature regimes in semiarid ecosystems. *Geoderma* **263**, 35–46. <https://doi.org/10.1016/j.geoderma.2015.09.012> (2016).
- Wu, Y. et al. Development of artificially induced biological soil crusts in fields and their effects on top soil. *Plant. Soil.* **370** (1–2), 115–124. <https://doi.org/10.1007/s11104-013-1611-6> (2013).
- Chock, T. et al. Responses of biological soil crusts to rehabilitation strategies. *J. Arid Environ.* **163**, 77–85. <https://doi.org/10.1016/j.jaridenv.2018.10.007> (2019).
- Xie, Z., Wang, Y., Liu, Y. & Liu, Y. Ultraviolet-B exposure induces photo-oxidative damage and subsequent repair strategies in a desert Cyanobacterium microcoleus vaginatus gom. *Eur. J. Soil. Biol.* **45**, 377–382. <https://doi.org/10.1016/j.ejsobi.2009.04.003> (2009).
- Rossi, F., Li, H., Liu, Y. & De Philippis, R. Cyanobacterial inoculation (cyanobacterisation): perspectives for the development of a standardized multifunctional technology for soil fertilization and desertification reversal. *Earth- Sci. Rev.* **171**, 28–43. <https://doi.org/10.1016/j.earscirev.2017.05.006> (2017).
- Mugnai, G. et al. The potential of the Cyanobacterium *Leptolyngbya ohadii* as inoculum for stabilizing bare sandy substrates. *Soil. Biol. Biochem.* **127**, 318–328. <https://doi.org/10.1016/j.soilbio.2018.08.007> (2018).
- Kheirfam, H., Sadeghi, S. H. R., Homaei, M. & Zarei Darki, B. Quality improvement of an erosion-prone soil through microbial enrichment. *Soil. Tillage Res.* **165**, 230–238. <https://doi.org/10.1016/j.still.2016.08.021> (2017a).
- Kheirfam, H., Sadeghi, S. H. R., Zarei Darki, B. & Homaei, M. Controlling rainfall-induced soil loss from small experimental containers through inoculation of bacteria and cyanobacteria. *Catena* **152**, 40–46. <https://doi.org/10.1016/j.catena.2017.01.006> (2017b).
- Muñoz-Rojas, M. et al. Cyanobacteria inoculation enhances carbon sequestration in soil substrates used in dryland restoration. *Sci. Total Environ.* **636**, 1149–1154. <https://doi.org/10.1016/j.scitotenv.2018.04.265> (2018).
- Kheirfam, H. Increasing soil potential for carbon sequestration using microbes from biological soil crusts. *J. Arid Environ.* **172**, 104022. <https://doi.org/10.1016/j.jaridenv.2019.104022> (2020).
- Kimural, K. & Okuro, T. Cyanobacterial biocrust on biomineralized soil mitigates freeze-thaw effects and preserves structure and ecological functions. *Microb. Ecol.* **87**, 69. <https://doi.org/10.1007/s00248-024-02389-w> (2024).
- Fick, S. E., Barger, N., Tatarko, J. & Duniway, M. C. Induced biological soil crust controls on wind erodibility and dust (PM10) emissions. *Earth Surf. Process. Land.* **45**, 224–236. <https://doi.org/10.1002/esp.4731> (2020).
- Park, C. H., Li, X. R., Jia, R. L. & Hur, J. S. Combined application of cyanobacteria with soil fixing chemicals for rapid induction of biological soil crust formation. *Arid Land. Res. Manag.* **31**, 81–93. <https://doi.org/10.1080/15324982.2016.1198842> (2017).
- Chandler, D. G., Day, N., Madsen, M. D. & Belnap, J. Amendments fail to hasten biocrust recovery or soil stability at a disturbed dryland sandy site. *Restor. Ecol.* **27**, 289–297. <https://doi.org/10.1111/rec.12870> (2019).
- Lan, S. & Rossi, F. Combination of chemical and cyanobacterial inoculation promotes biocrust development: A novel perspective for combating desertification. *ACS Sustain. Chem. Eng.* **9**, 9506–9507. <https://doi.org/10.1021/ACSUSCHEMENG.1C02856> (2021).

26. Yang, K., Wang, X. L., Cheng, H. F. & Tao, S. Effect of aging on stabilization of cd and Ni by biochars and enzyme activities in a historically contaminated alkaline agricultural soil simulated with wet-dry and freeze-thaw cycling. *Environ. Pollut.* **268**, 115846. <https://doi.org/10.1016/j.envpol.2020.115846> (2021).
27. Lu, S. G., Sun, F. F. & Zong, Y. T. Effect of rice husk Biochar and coal fly Ash on some physical properties of expansive clayey soil (Vertisol). *Catena* **114**(2), 37–44. <https://doi.org/10.1016/j.catena.2013.10.014> (2014).
28. Zhao, D., Huang, S. & Huang, J. S. Effects of Biochar on hydraulic parameters and shrinkage-swelling rate of silty clay. *Trans. Chin. Soc. Agric. Eng.* **31**(17), 136–143. <https://doi.org/10.11975/j.issn.1002-6819.2015.17.018> (2015).
29. Glab, T., Palmowska, J. & Zaleski, T. Effect of Biochar application on soil hydrological properties and physical quality of sandy soil. *Geoderma* **281**, 11–20. <https://doi.org/10.1016/j.geoderma.2016.06.028> (2016).
30. Wang, Z. et al. Wind erosion control of bare surface soil in arid mining area by cyanobacterial inoculation and Biochar amendment. *Catena* **250**, 108765. <https://doi.org/10.1016/j.catena.2025.108765> (2025).
31. Wang, W. B., Shu, X., Zhang, Q. F. & Guénou, R. Effects of freeze–thaw cycles on the soil nutrient balances, infiltration, and stability of cyanobacterial soil crusts in Northern China. *Plant. Soil.* **386**, 263–272. <https://doi.org/10.1007/s11104-014-2263-x> (2015).
32. Mellander, P. E., Lofvenius, M. O. & Laudon, H. Climate change impact on snow and soil temperature in boreal Scots pine stands. *Clim. Chang.* **85**, 179–193. (2007). <https://doi.org/10.1007/s10584-007-9254-3>.
33. Sahin, U., Angin, I., Kiziloglu, F. M., 2008. Effect of freezing and thawing processes on some physical properties of saline–sodic soils mixed with sewage sludge or fly ash. *Soil Tillage Res.* **99**, 254–260. <https://doi.org/10.1016/j.still.2008.03.001>.
34. Viklander, P. & Eigenbrod, D. Stone movements and permeability change in till caused by freezing and thawing. *Cold Reg. Sci. Technol.* **31**, 151–162. [https://doi.org/10.1016/S0165-232X\(00\)00009-4/](https://doi.org/10.1016/S0165-232X(00)00009-4/) (2000).
35. Chen, J., Zheng, X., Zang, H., Liu, P. & Sun, M. Numerical simulation of moisture and heat coupled migration in seasonal freeze–thaw soil media. *J. Pure Appl. Microbiol.* **7**, 151–156.
36. Zhang, Z., Pendin, V. V., Feng, W. J., Zhang, Z. Q., 2015. The influence of freeze–thaw cycles on the granulometric composition of Moscow morainic clay. *Sci. Cold Arid. Reg.* **7**, 199–205. (2013). <https://doi.org/10.3724/SP.J.1226.2015.00199>
37. Shen, S. W., Xia, C. C. & Huang, J. H. Influence of seasonal melt layer depth on the stability of surrounding rock in permafrost regions based on the measurement. *Nat. Hazards* **75**(3), 2545–2557. <https://doi.org/10.1007/s11069-014-1442-7> (2015).
38. Güllü, H. & Khudir, A. Effect of freeze–thaw cycles on unconfined compressive strength of fine-grained soil treated with jute fiber, steel fiber and lime. *Cold Reg. Sci. Technol.* **106–107**, 55–65. <https://doi.org/10.1016/j.coldregions.2014.06.008> (2014).
39. Mohanty, S. K., Saiters, J. E. & Ryan, J. N. Colloid-facilitated mobilization of metals by freeze–thaw cycles. *Environ. Sci. Technol.* **48**, 977–984. <https://doi.org/10.1021/es403698u> (2014).
40. Song, Y., Zou, Y., Wang, G. & Yu, X. Altered soil carbon and nitrogen cycles due to the freeze–thaw effect: A meta-analysis. *Soil. Biol. Biochem.* **109**, 35–49. <https://doi.org/10.1016/j.soilbio.2017.01.020> (2017).
41. Zhao, R. M., Hui, R., Liu, L. C., Xie, M. & An, L. Z. Effects of snowfall depth on soil physical–chemical properties and soil microbial biomass in moss-dominated crusts in the Gurbantunggut desert, Northern China. *Catena* **169**, 175–182. <https://doi.org/10.1016/j.catena.2018.05.042> (2018).
42. Hui, R. et al. Changes in winter snow depth affects photosynthesis and physiological characteristics of biological soil crusts in the Tengger desert. *Photosynthetica* **56**(4), 1304–1312. <https://doi.org/10.1007/s11099-018-0838-0> (2018).
43. Wang, Y. B. et al. Freeze–thaw cycles aggravated the negative effects of moss–biocrusts on hydraulic conductivity in sandy land. *Catena* **207**, 105638. <https://doi.org/10.1016/j.catena.2021.105638> (2021).
44. Zhang, Q. et al. Differentiate responses of soil nutrient levels and enzymatic activities to freeze–thawing cycles in different layers of moss-dominated biocrusts in a temperate desert. *Front. Plant. Sci.* **14**, 1137754. <https://doi.org/10.3389/fpls.2023.1137754> (2023b).
45. Zuo, Y. T. et al. Effect of Biochar application on freezing–thawing deformation of farmland soil during freeze–thaw cycling. *Geoderma* **405**, 115510. <https://doi.org/10.1016/j.geoderma.2021.115510> (2022).
46. Xiu, L. et al. Effects of biochar and straw returning on the key cultivation limitations of Albic soil and soybean growth over 2 years. *Catena* **173**, 481–493. (2019). <https://doi.org/10.1016/j.catena.2018.10.041>.
47. Li, G. Y., Fan, H. M., 2014. Effect of freeze–thaw on water stability of aggregates in a black soil of northeast China. *Pedosphere* **24**, 285–290. [https://doi.org/10.1016/S1002-0160\(14\)60015-1](https://doi.org/10.1016/S1002-0160(14)60015-1).
48. Dubey, A. A. et al. Experimental investigation to mitigate aeolian erosion via biocementation employed with a novel ureolytic soil isolate. *Aeolian Res.* **52**, 100727. <https://doi.org/10.1016/j.aeolia.2021.100727> (2021).
49. Song, C. Y. et al. Preparation of microbial dust suppressant and its application in coal dust suppression. *Adv. Powder Technol.* **32**, 4509–4521. <https://doi.org/10.1016/j.apt.2021.10.001> (2021).
50. Nafees Ahmad, H. M. et al. Modeling sediment and nitrogen export from a rural watershed in Eastern Canada using the soil and water assessment tool. *J. Environ. Qual.* **40**(4), 1182–1194. <https://doi.org/10.2134/jeq2010.0530> (2011).
51. Al-Kaisi, M. M., Douelle, A. & Kwaw-Mensah, D. Soil microaggregate and macroaggregate decay over time and soil carbon change as influenced by different tillage systems. *J. Soil. Water Conserv.* **69**(6), 574–580. <https://doi.org/10.2489/jswc.69.6.574> (2014).
52. Negis, H., Seker, C., Gumus, I. & Erçi, V. Establishment of a minimum dataset and soil quality assessment for multiple reclaimed areas on a wind-eroded region. *Catena* **229**, 107208. <https://doi.org/10.1016/j.catena.2023.107208> (2023).
53. Shahabinejad, N., Mahmoodabadi, M., Jalalian, A. & Chavoshi, E. In situ field measurement of wind erosion and threshold velocity in relation to soil properties in arid and semiarid environments. *Environ. Earth Sci.* **78**, 501. <https://doi.org/10.1007/s12666-019-0193-0> (2019).
54. Giuffrida, F., Carla, C., Angelo, M. & Cherubino, L. Effects of salt stress imposed during two growth phases on cauliflower production and quality. *J. Sci. Food Agri.* **97**, 1552–1560. <https://doi.org/10.1002/jsfa.7900> (2016).
55. Han, Y., Zhao, W. W., Ding, J. Y. & Ferreira, C. S. S. Soil erodibility for water and wind erosion and its relationship to vegetation and soil properties in China's drylands. *Sci. Total Environ.* **903**, 166639. <https://doi.org/10.1016/j.scitotenv.2023.166639> (2023).
56. Zanganeh, F., Heidari, A., Sepehr, A. & Rohani, A. Bioaugmentation and bioaugmentation-assisted phytoremediation of heavy metal contaminated soil by a synergistic effect of cyanobacteria inoculation, Biochar, and purslane (*Portulaca Oleracea* L.). *Environ. Sci. Pollut. R.* **29**(4), 6040–6059. <https://doi.org/10.1007/s11356-021-16061-0> (2022).
57. Wei, B. L. et al. Soil pH restricts the ability of Biochar to passivate cadmium: A meta-analysis. *Environ. Res.* **219**, 115110. <https://doi.org/10.1016/j.envres.2022.115110> (2023).
58. Lin, Q. Y. et al. Assessing the potential of Biochar and aged Biochar to alleviate aluminum toxicity in an acid soil for achieving cabbage productivity. *Ecotox Environ. Safe* **161**, 290–295. <https://doi.org/10.1016/j.ecoenv.2018.06.010> (2018).
59. Rechberger, M. V. et al. Enhanced Cu and cd sorption after soil aging of woodchip-derived Biochar: What were the driving factors? *Chemosphere* **216**, 463–471. <https://doi.org/10.1016/j.chemosphere.2018.10.094> (2018).
60. Freppaz, M., Williams, B. L., Edwards, A. C., Scalenghe, R. & Zanini, E. Simulating soil freeze/thaw cycles typical of winter alpine conditions: Implications for N and P availability. *Appl. Soil. Ecol.* **35**(1), 247–255. <https://doi.org/10.1016/j.apsoil.2006.03.012> (2007).
61. Lawrinenko, M., Laird, D. A., Johnson, R. L. & Jing, D. P. Accelerated aging of Biochars: Impact on anion exchange capacity. *Carbon* **103**, 217–227. <https://doi.org/10.1016/j.carbon.2016.02.096> (2016).
62. Xu, Z. B., Xu, X. Y., Tsang, D. C. W. & Cao, X. D. Contrasting impacts of pre- and post-application aging of Biochar on the immobilization of cd in contaminated soils. *Environ. Pollut.* **242**, 1362–1370. <https://doi.org/10.1016/j.envpol.2018.08.012> (2018).
63. Li, Z. H. et al. Synergistic effect of cyanobacteria and nano-sand-stabilizer on biocrust formation and sand fixation. *J. Environ. Chem. Eng.* **9**(1), 104887. <https://doi.org/10.1016/j.jece.2020.104887> (2021).
64. Brodowski, S., John, B., Flessa, H. & Amelung, W. Aggregate-occluded black carbon in soil. *Eur. J. Soil. Sci.* **57**(4), 539–546. <https://doi.org/10.1111/j.1365-2389.2006.00807.x> (2006).

65. Zhang, L., Ren, F. P., Li, H., Cheng, D. B. & Sun, B. Y. The influence mechanism of freeze-thaw on soil erosion: A review. *Water* **13**, 1010. <https://doi.org/10.3390/w13081010> (2021).
66. Kreyling, J., Beierkuhnlein, C. & Jentsch, A. Effects of soil freeze-thaw cycles differ between experimental plant communities. *Basic. Appl. Ecol.* **11**, 65–75. <https://doi.org/10.1016/j.baec.2009.07.008> (2010).
67. Sun, J. N. et al. Contrasting effects of corn straw Biochar on soil water infiltration and retention at tilled and compacted bulk densities in the yellow river delta. *Can. J. Soil. Sci.* **99**, 357–366. <https://doi.org/10.1139/cjss-2019-0004> (2019).
68. Guo, R. et al. Interactive effects of maize straw-derived Biochar and N fertilization on soil bulk density and porosity, maize productivity and nitrogen use efficiency in arid areas. *J. Soil. Sci. Plant. Nut.* **22**(4), 4566–4586. <https://doi.org/10.1007/s42729-022-00881-1> (2022).
69. Obia, A., Mulder, J., Martinsen, V., Cornelissen, G. & Borresen, T. In situ effects of Biochar on aggregation, water retention and porosity in light-textured tropical soils. *Soil. Till. Res.* **155**, 35–44. <https://doi.org/10.1016/j.still.2015.08.002> (2016).
70. Kakeh, J. et al. Biological soil crusts determine soil properties and salt dynamics under arid Climatic condition in Qara Qir, Iran. *Sci. Total Environ.* **732**, 139168. <https://doi.org/10.1016/j.scitotenv.2020.139168> (2020).
71. Lu, J., Sun, B., Ren, F., Li, H. & Jiao, X. Effect of freeze-thaw cycles on soil detachment capacities of three loamy soils on the loess plateau of China. *Water* **13**(3), 342. <https://doi.org/10.3390/w13030342> (2021).
72. Liu, T., Xu, X. & Yang, J. Experimental study on the effect of freezing-thawing cycles on wind erosion of black soil in Northeast China. *Cold Reg. Sci. Technol.* **136**, 1–8. <https://doi.org/10.1016/j.coldregions.2017.01.002> (2017).
73. Ren, X., Sun, H., Wang, F., Zhang, P. & Zhu, H. K. Effect of aging in field soil on Biochar's properties and its sorption capacity. *Environ. Pollut.* **242**, 1880–1886. <https://doi.org/10.1016/j.envpol.2018.07.078> (2018).
74. He, Z. et al. Evolution mechanism of soil hydrothermal parameters under freeze-thaw cycles: Regulatory significance of straw and Biochar. *J. Clean. Prod.* **385**, 135787. <https://doi.org/10.1016/j.jclepro.2022.135787> (2023).
75. Kim, Y. J., Kim, J. & Jung, J. Y. Responses of dissolved organic carbon to freeze-thaw cycles associated with the changes in microbial activity and soil structure. *Cryosphere* **17**, 3101–3114. <https://doi.org/10.5194/tc-17-3101-2023> (2023).
76. Dong, C. et al. Effects of freeze-thaw cycles on the size distribution and stability of soil aggregate in the permafrost regions of the Qinghai-Tibetan plateau. *Environ. Res. Commun.* **5** (9), 095008. <https://doi.org/10.1088/2515-7620/acfd8b> (2023).
77. Zhang, Z., Wei, M. A., Feng, W., Xiao, D. & Hou, X. Reconstruction of soil particle composition during freeze-thaw cycling: A review. *Pedosphere* **26**, 167–179. [https://doi.org/10.1016/S1002-0160\(15\)60033-9](https://doi.org/10.1016/S1002-0160(15)60033-9) (2016).
78. Zhai, J. et al. Experimental study on the effect of freeze-thaw cycles on the mineral particle fragmentation and aggregation with different soil types. *Minerals* **11**, 913. <https://doi.org/10.3390/min11090913> (2021).
79. Gao, D. et al. Responses of terrestrial nitrogen pools and dynamics to different patterns of freeze-thaw cycle: A meta-analysis. *Global Change Biol.* **24**(6), 2377–2389. <https://doi.org/10.1111/gcb.14010> (2018).
80. Zhang, Y. Q. et al. Soil environment, carbon and nitrogen cycle functional genes in response to freeze-thaw cycles and Biochar. *J. Clean. Prod.* **444**, 141345. <https://doi.org/10.1016/j.jclepro.2024.141345> (2024).
81. Oztas, T. & Fayetorbay, F. Effect of freezing and thawing processes on soil aggregate stability. *Catena* **52**(1), 1–8. [https://doi.org/10.1016/S0341-8162\(02\)00177-7](https://doi.org/10.1016/S0341-8162(02)00177-7) (2003).
82. Tierney, G. L. et al. Soil freezing alters fine root dynamics in a Northern hardwood forest. *Biogeochemistry* **56**(2), 175–190. <https://doi.org/10.1023/A:1013072519889> (2001).
83. Bernard, L. et al. Advancing the mechanistic Understanding of the priming effect on soil organic matter mineralization. *Funct. Ecol.* **36**, 1355–1377. <https://doi.org/10.1111/1365-2435.14038> (2022).
84. Xie, S. B., Qu, J. J., Xu, X. T. & Pang, Y. J. Interactions between freeze-thaw actions, wind erosion desertification, and permafrost in the Qinghai-Tibet plateau. *Nat. Hazards* **85**, 829–850. <https://doi.org/10.1007/s11069-016-2606-4> (2017).
85. Fattahi, S. M., Soroush, A. & Huang, N. Wind erosion control using inoculation of aeolian sand with cyanobacteria. *Land. Degrad. Dev.* **31**(15), 2104–2116. <https://doi.org/10.1002/ldr.3590> (2020).
86. Zhang, Q. et al. Effects of Biochar amendment on soil thermal conductivity, reflectance, and temperature. *Soil. Sci. Soc. Am. J.* **77**(5), 1478. <https://doi.org/10.2136/sssaj2012.0180> (2013).
87. Liu, Z., Xu, J., Li, X. & Wang, J. Mechanisms of Biochar effects on thermal properties of red soil in South China. *Geoderma* **323**, 41–51. <https://doi.org/10.1016/j.geoderma.2018.02.045> (2018).
88. Mager, D. M. Carbohydrates in cyanobacterial soil crusts as a source of carbon in the Southwest Kalahari, Botswana. *Soil. Biol. Biochem.* **42**(2), 313–318. <https://doi.org/10.1016/j.soilbio.2009.11.009> (2010).
89. Lan, S., Wu, L., Zhang, D. & Liu, Y. Effects of drought and salt stresses on man-made cyanobacterial crusts. *Eur. J. Soil. Biol.* **46**(6), 381–386. <https://doi.org/10.1016/j.ejsobi.2010.08.002> (2010).
90. Zhou, X., Tao, Y., Yin, B., Tucker, C. & Zhang, Y. Nitrogen pools in soil covered by biological soil crusts of different successional stages in a temperate desert in central Asia. *Geoderma* **366**, 114166. <https://doi.org/10.1016/j.geoderma.2019.114166> (2019).
91. Gao, L. et al. Biological soil crusts decrease erodibility by modifying inherent soil properties on the loess plateau, China. *Soil. Biol. Biochem.* **105**, 49–58. <https://doi.org/10.1016/j.soilbio.2016.11.009> (2017).
92. Chen, X. H. & Duan, Z. H. Impacts of soil crusts on soil physicochemical characteristics in different rainfall zones of the arid and semi-arid desert regions of Northern China. *Environ. Earth Sci.* **73**, 3335e3347. <https://doi.org/10.1007/s12665-014-3622-x> (2015).
93. Wu, J. et al. Effects of combined application of chemical fertilizer and Biochar on soil physio-biochemical properties and maize yield. *Agriculture* **13**(6), 1200. <https://doi.org/10.3390/agriculture13061200> (2023).
94. Liu, B. et al. Linking soil water retention capacity to pore structure characteristics based on X-ray computed tomography: Chinese Mollisol under freeze-thaw effect. *Geoderma* **401**, 115170. <https://doi.org/10.1016/j.geoderma.2021.115170> (2021).
95. Shen, Q., Wu, M. J. & Zhang, M. K. Accumulation and relationship of metals in different soil aggregate fractions along soil profiles. *J. Environ. Sci.* **115**, 47–54. <https://doi.org/10.1016/j.jes.2021.07.007> (2022).
96. Zhao, Y. D. & Hu, X. A pore-scale investigation of soil aggregate structure responding to freeze-thaw cycles using x-ray computed microtomography. *J. Soils Sediments* **23**, 3137–3148. <https://doi.org/10.1007/s11368-023-03539-2> (2023).
97. Sun, Z. C. et al. Biochar altered native soil organic carbon by changing soil aggregate size distribution and native SOC in aggregates based on an 8-year field experiment. *Sci. Total Environ.* **708**, 13482. <https://doi.org/10.1016/j.scitotenv.2019.134829> (2019b).
98. Ji, L. L., Tan, W. F. & Chen, X. H. Arbuscular mycorrhizal mycelial networks and glomalin-related soil protein increase soil aggregation in calcaric regosol under well-watered and drought stress conditions. *Soil. Till. Res.* **185**, 1–8. <https://doi.org/10.1016/j.still.2018.08.010> (2019).
99. Wang, Z. et al. Montmorillonite combined with microbially induced carbonate precipitation for wind erosion control of bare surface soil in arid mining area. *Process. Saf. Environ.* **187**, 926–939. <https://doi.org/10.1016/j.psep.2024.05.015> (2024).

Acknowledgements

This work was supported by the National Science Foundation of China (52264013), Inner Mongolia Science & Technology Plan Program (2020), the basic research funds for universities directly under the Inner Mongolia Autonomous Region (2023CXPT004), the National Key Research and Development Program of China (2023YFF1306003), and Inner Mongolia Engineering Research Center of Evaluation and Restoration in the Mining Ecological Environment.

Author contributions

Zhe Wang: Conceptualization, Supervision, Writing-review & editing, Funding acquisition, Project administration. Xueshi Liu: Formal analysis, Data curation, Writing- original draft. Fenghui Sun: Supervision, Conceptualization.: Formal analysis, Data curation. Qinghong Jiang: Formal analysis. Haili Shang: Formal analysis. Chunli Zheng: Supervision, Conceptualization, Funding acquisition.

Declarations

Competing interests

The authors declare no competing interests.

Additional information

Supplementary Information The online version contains supplementary material available at <https://doi.org/10.1038/s41598-025-96688-y>.

Correspondence and requests for materials should be addressed to Q.J.

Reprints and permissions information is available at www.nature.com/reprints.

Publisher's note Springer Nature remains neutral with regard to jurisdictional claims in published maps and institutional affiliations.

Open Access This article is licensed under a Creative Commons Attribution-NonCommercial-NoDerivatives 4.0 International License, which permits any non-commercial use, sharing, distribution and reproduction in any medium or format, as long as you give appropriate credit to the original author(s) and the source, provide a link to the Creative Commons licence, and indicate if you modified the licensed material. You do not have permission under this licence to share adapted material derived from this article or parts of it. The images or other third party material in this article are included in the article's Creative Commons licence, unless indicated otherwise in a credit line to the material. If material is not included in the article's Creative Commons licence and your intended use is not permitted by statutory regulation or exceeds the permitted use, you will need to obtain permission directly from the copyright holder. To view a copy of this licence, visit <http://creativecommons.org/licenses/by-nc-nd/4.0/>.

© The Author(s) 2025